Anthropocene tipping point reverses long-term Holocene cooling of the Mediterranean Sea

Nick Marriner, David Kaniewski, Majid Pourkerman, Benoît Devillers

Anthropocene tipping point reverses long-term Holocene cooling of the Mediterranean Sea: a meta-analysis of the basin's Sea Surface Temperature records

Nick Marriner[1*†], David Kaniewski[2,3†], Majid Pourkerman[4] & Benoît Devillers[5,6]

[1]CNRS, ThéMA, Université de Franche-Comté, UMR 6049, MSHE Ledoux, 32 rue Mégevand, 25030 10 Besançon Cedex, France

*Corresponding author. Email: nick.marriner@univ-fcomte.fr

[2]TRACES, UMR 5608 CNRS, Université Toulouse Jean Jaurès, Maison de la Recherche, 5 allées A. Machado 12 31058 Toulouse Cedex 9, France

[3]Université Paul Sabatier-Toulouse 3, Département Biologie et Géosciences, 118 Route de Narbonne, 31062 Toulouse cedex 9, France

[4]Iranian National Institute for Oceanography and Atmospheric Sciences (INIOAS), 3 Etemad Zadeh St., Fatemi Ave., 14155-4781 Tehran, Iran

[5]Université Paul-Valéry - Montpellier 3, CNRS, MC, UMR 5140 Archéologie des sociétés méditerranéennes, 34000, Montpellier, France

[6]Labex ARCHIMEDE, ANR-11-LABX-0032-01, Université Paul-Valery, Montpellier 3, Route de Mende, 34199 Montpellier Cedex 05, France

† These authors contributed equally to this work

Abstract

The Mediterranean is facing numerous socio-environmental challenges linked to global change, frequently compounded by rapid population growth. Within this framework, regional-scale Holocene temperature reconstructions are key to placing industrial-era warming into the perspective of natural climatic variability. Here, we present a new Mediterranean Sea Surface Temperature (SST) stack based on 54 records for the last 11,750 years, to evaluate millennial-to-centennial-scale climate variability and to contextualize present and future changes. The Holocene thermal maximum is reconstructed 9,400–3,000 years ago and is estimated to have been an average of 0.47 ± 0.2°C warmer than the mean for 1900-1960, followed by the onset of long-term cooling beginning around 3000 years BP. The coolest temperatures during the last ten millennia are recorded during the Little Ice Age. We find that Mediterranean Sea temperatures have risen from near the coldest to warmest

levels of the Holocene within the past century, with decadal warming rates that are ~16 times greater than the closest interglacial analogue. The basin's SSTs have consistently exceeded the full distribution of Holocene warmth since 2011.

Keywords: Sea Surface Temperatures, Holocene, Mediterranean, Anthropocene.

Introduction

The Mediterranean comprises one of the world's most prominent and vulnerable climate change "hotspots" due to its rapid response to atmospheric forcings (Tuel and Eltahir, 2020); current change and future scenarios consistently highlight the substantial and growing risks that the basin will face in coming decades (Guiot and Cramer, 2016; Tramblay et al., 2020). Within this context, Sea Surface Temperature (SST) is an important component of the Mediterranean climate system (Macias et al., 2013) and knowledge of past, present and future trends in its SSTs is crucial for future climate scenarios and to improve understanding of thermal and dynamical interactions between the Mediterranean Sea, the atmosphere (Alexander et al., 2018; Pastor et al., 2018) and steric-driven sea-level changes (Vacchi et al., 2021).

Climate change constitutes one of multiple drivers affecting Mediterranean anthroposcapes and human health (Cramer et al., 2018), either directly (e.g. through temperature extremes, drought and water security, storms) or indirectly (modifications in food provision and quality, air pollution, creation of urban heat islands). Future warming in the Mediterranean region is forecasted to exceed global rates by 25 %, with summer warming outpacing the global mean by 40 % (Lionello and Scarascia, 2018). In 2019, Mediterranean countries hosted >520 million people (United Nations, 2019) and population exposure to heat is increasing due to climate change and rapid rates of urbanization. For example, from 2000-2019, >65,000 people died due to Mediterranean heatwaves (EM-DAT, 2020). This figure is particularly alarming because the frequency of Mediterranean heatwave days is projected to evolve from an average of about two days per summer for the period 1961–1990 to around 13 days for 2021–2050 and 40 days for 2071–2100 (Fischer and Schär, 2010). The Mediterranean coastline, in particular, is extremely sensitive

to heatwaves and strong changes in ambient temperature and sea temperatures, notably the basin's densely populated urban centers.

Mediterranean SST data covering the Holocene can furnish crucial insight into natural decadal to centennial time-scale changes and put recent climate change into a longer-term perspective (McGregor et al., 2015; Abram et al., 2016). This is particularly important because semi-enclosed basins like the Mediterranean Sea are poorly resolved by the ~1° resolution of many global climate models. The Mediterranean's rich archaeological record also emphasizes the importance of recurring socio-cultural changes/transitions and demonstrates that the region's past societies faced climate-related challenges at various points during the Holocene (Kaniewski et al., 2017). Here, we place today's regional SST changes into the broader temporal context of the Holocene using a consistent framework based on spatially averaged estimates of Mediterranean SSTs. Mediterranean Sea temperatures are now ~1.4°C higher than at the turn of the 20th century, compared with an increase of ~1.2°C worldwide (NOAA, 2020). Understanding future trends in SSTs is, therefore, of paramount importance for Mediterranean climate adaptation policies, including public health, land-use and the conservation of biodiversity.

Methods

The SST database gathers 54 records from 44 locations in the Mediterranean Sea (see **Table 1**). **Figure 1** displays the spatial distribution of the archives used in the database. The records derive from marine cores and are based on the following proxy methods (**Figures S1 and S2**): alkenones (n=34), long-chain diols (n=2), Mg/Ca (n=11), TEX86 (n=5), δ18Ow foraminifera (n=1) and Ri OH-GDGTs (n=1). They range in temporal length from 0 to 244,350 years BP, but only the Holocene section of each record was retained for the database. Details regarding the collection, analysis and interpretation of individual records are provided in the original publications. A list of sites in the database, including basic metadata, is presented in **Table 1**. To facilitate comparison of information on a common chronological grid and for shared spectral resolutions, all records were annualized using nearest-neighbor interpolation. Each initial record was converted into SST anomalies (in °C) by subtracting the mean temperature from each sequence. This method also helps to reduce analytical biases associated with individual geochemical reconstruction

techniques. The time series were subsequently summed and averaged to generate a spatially averaged Holocene record of Mediterranean SSTs. To quantify analytical uncertainties in the time series, we calculated Confidence Intervals, integrating the number of records at a given point in time, the reconstructed annual mean and the associated standard deviation (**Figure S3**). The mean CI for the entire time series is 0.23°C. We also incorporated the varying chronological uncertainties (2σ) associated with each of the 54 time series used to construct the SST stack, by means of the initial age models. **Figure S4** plots the 2σ error average of all records used to construct the SST record for each time point. The data are plotted at a resolution of 50 years for clarity. Mediterranean SSTs for 1854-2019 were extracted from the International Comprehensive Ocean-Atmosphere Data Set (ICOADS) (https://icoads.noaa.gov; 55). All SST data are reported as average temperature anomalies. For data plotted on the B2K timescale, the year 2000 CE represents 0. Negative time values are post-2000 (e.g. 2010 = -10).

To quantify the potential role of geographic location in influencing the overall signal we applied the following three-step analysis. (1) The initial 54 records were divided into three separate entities East (21°E to 36°E), Central (10°E to 20.9999°E) and West (-4.7496°W to 9.9999°E) Mediterranean. The SST data were transformed into percentages of the total signal. For each calculation, the mean was subtracted by geographic entity using these percentages. (2) Next, we took the number of sequences by geographic entity (East, Central and West) and transformed these numbers into percentages of the total signal. For each calculation, we also subtracted the mean (per geographic entity) using these percentages. (3) To weight the overall signal using the three different zones, we multiplied the percentages produced in step 1 with those from step 2. The level of signal variation is low, with the exception of the first ~200 years of the Holocene, giving us confidence in the overall quality of the SST stack as a robust palaeoclimate record (**Figure S5**).

A homogeneity test was applied to the Holocene record of SSTs to detect shifts in the long-term dynamics. Each discordant period was categorized and its average indicated by “mu” (**Figure 2**). A polynomial regression was then applied (**Figure 2**) and a sinusoidal regression was calculated to model potential periodicities in the time series. The link between insolation and Mediterranean SSTs was tested, ranking the

insolation scores in ascending order and retaining the associated SST values. Averages were calculated and are plotted with their standard deviations (**Figure 3**). The same process was applied in testing the relationship between the Agassiz Ice Cap melt record and the SSTs (**Figure 4A-B**). Warming and cooling phases during the Holocene (expressed in °C per decade; **Figures 5-7**) were calculated by selecting the highest and lowest values for each climate episode. Rates were defined by subtracting the high and low values and dividing by time. A linear model was applied to present-day values to project warming values up to 2100, based on each of the past Holocene scenarios (with the associated standard deviation; **Figure 7E**).

A short-time Fourier transform was applied to the last two millennia (window = rectangle; **Figure S7**) to determine the sinusoidal frequency and the phase content of sections of the SST signal over time. Boxplots of Mediterranean SST variability during the Holocene (**Figure S8**) were plotted to highlight the extent of Global Warming since the 19th century AD. Each chronological window was defined by a series of homogeneity tests.

All of the raw data tables used to draft the figures are reported in the Excel file (Supplementary Material) accompanying the manuscript.

Results and discussion

Holocene evolution of Mediterranean SSTs

Figure 2 plots average SST anomalies on the B2K timescale. The record has successfully captured both first- and second-order pacemakers. Change-point analyses highlight three statistically significant periods. (1) The reconstruction shows a strong SST warming trend between 11,700 to 9400 B2K characterized by warming of ~2.8°C at an average rate of 0.12°C per century. The temperature anomalies range from -2.75 ± 0.59°C to 0.03 ± 0.26°C with a mean of -1.02 ± 0.39°C. This early Holocene period was characterized by a much greater range of variability than seen over later millennia. (2) Around 9400 years ago, the rates of SST change slowed rapidly. Between 9400 to 3000 B2K, temperatures plateaued in a phase of sustained warming with SST anomalies ranging from -0.01 ± 0.2°C to 0.58 ± 0.18°C, with an average anomaly of 0.32 ± 0.2°C. Maxima in the SST data occur at 4700-4950 B2K (average = 0.53 ± 0.23°C) and 7100-7200 B2K (average = 0.54 ± 0.19°C). (3) After

3000 BP, the reconstruction manifests an overall cooling trend of >1°C, from a maximum of 0.3 ± 0.19°C at 3000 B2K to a minimum of -0.77 ± 0.06°C at 110 B2K.

Following the disappearance of the major Northern Hemisphere ice sheets between 8000 B2K and 6000 B2K, the chief SST trends in the Mediterranean parallel the dominant climate forcings of the Holocene. Mediterranean SSTs during the last 8000 years are characterized by an overall decrease in temperatures, consistent with insolation forcing associated with decreasing orbital obliquity. The strongly decreasing boreal summer insolation induced a progressive SST cooling of ~1.4°C (**Figure 3**). A southerly zonal shift in the mean position of the intertropical convergence zone (ITCZ; Schneider et al., 2014) allowed an expansion of the Siberian High over Eurasia, ultimately resulting in cooler, drier winters and springs in the Mediterranean (Peyron et al., 2017). Our reconstruction demonstrates that cooling only became well expressed in the past three millennia, accompanied by a marked transition in seasonality that is clearly attested in terrestrial records from around the Mediterranean, concomitant with a gradual precession-driven decrease in summer insolation versus increases in winter values (Peyron et al., 2011; Kaniewski et al., 2020).

Superimposed on the insolation-based Holocene cooling of Mediterranean SSTs, the reconstruction manifests considerable variability linked to second-order forcing agents. Six periods of marked SST cooling are delineated at 8360-8100 B2K, 5400-5100 B2K, 4220-3900 B2K, 3130-2800 B2K, 1470-1250 B2K and 670-140 B2K (**Figures 4 and 5**). Our analysis shows that these rapid Mediterranean cooling phases mesh with internal oceanic shifts in the North Atlantic during which ice rafting and meltwater outburst events from Greenland and North America cooled and freshened ocean surface waters, slowing and modifying the geography of deep-water formation and disrupting the northerly transport of warm low-latitude waters by the thermohaline circulation (Fisher et al., 2012; **Figure 4**). These major changes in the Atlantic Meridional Overturning Circulation (AMOC) significantly affected SSTs in the Mediterranean with broader implications for the basin's palaeoclimates (Fletcher et al., 2013). Terrestrial-based records demonstrate that the cooling phases were frequently associated with reductions in precipitation and temperatures, and had wider social, cultural, and political consequences for some Mediterranean and West

Asian societies at key points during the mid to late Holocene (Weiss, 2016; Sinha et al., 2019). For instance, the Late Bronze Age to Early Iron Age transition in the Eastern Mediterranean was characterized by a 30-40% reduction in precipitation which appears to have engendered food shortages in parts of the Levant, Egypt and Greece, and marked the onset of the Iron Age Dark Ages (Kaniewski et al., 2013; Kaniewski et al., 2017). The archaeological record documents significant cultural and socio-economic shifts in the Levant and Egypt during the Late Bronze Age, and several sites from Syria, Israel and the Nile Delta show a transition to cooler and more arid conditions at ~1200 BC (Kaniewski et al., 2019). Egypt withdrew from its province in Canaan and experienced food shortages (Shaw, 2004). In Greece, the population was reduced, and the world of organized state armies, kings, officials, and redistributive systems disappeared. During the Early Iron Age, Greece was divided into independent regions organized by kinship groups and the oikoi or households, the origins of the later poleis. This model appears to have provided citizens with greater opportunities for political participation and rendered these societies more resilient to climate change. Later, around 1500-1250 B2K, rapid climate cooling of 0.27°C coincided with the transformation of the eastern Roman empire into the Byzantine empire (Büntgen et al., 2016) and marked the end of a period of relatively stable climatic conditions during which Rome extended its hegemony over great swathes of Europe, the Near East and North Africa.

The lowest SSTs during the past 10,000 years occurred during the 1600 to 1800s. At this time, many Mediterranean glaciers attained their maximum Holocene extent and even existed as far south as the High Atlas of Morocco and the Sierra Nevada of southern Spain (Hughes, 2018). All of the solar minima of the Little Ice Age are clearly captured by the Mediterranean SST stack. These cold episodes mesh with abrupt cooling events in the Bosphorus and colder winters in Istanbul (Turkey), both identified in historical data (Yavuz et al., 2007; **Figure S7**). Rapid temperature deviations are therefore important in fully comprehending the complex interplay between Mediterranean climate, landscapes and its societies.

Climate change is not only manifest in mean SST trends but also in shifts in the anatomy of past abrupt warmings and coolings recorded in the Mediterranean SST stack. We probed the duration and amplitude of cooling/warming transitions in the

SST record, focusing on four warming phases and nine cooling episodes (**Figure 6**). We note large variability in the transition duration from one event to the other. The longest warming transition was for the Holocene Warm Period with a warming of 0.43 ± 0.17°C over ~510 years. The longest cooling-phase transition was the 3.2 Event characterized by cooling of -0.38 ± 0.19°C over ~320 years which contrasts markedly with the short cooling-phase transition during the Dalton Minimum of the Little Ice Age with cooling of -0.45 ± 0.23°C in just ~45 years. The absence of a systematic pattern in the duration of SST transitions could result from internal climate variability superimposed on broader forcing mechanisms. Nonetheless, our data do suggest that warming and cooling phases have been particularly rapid and of high amplitude during the past 1000 years.

Present and future SSTs trends and implications

Our results demonstrate that the mean of Mediterranean SSTs for the decade 2010–2019 exceeds the warmest temperatures of the early to mid-Holocene (9000 to 3000 BP) by 0.31 ± 0.09°C. By contrast, the decadal SST mean of the early 20th century (1900–1909) was cooler than 86% of the Holocene distribution. Mediterranean SSTs have therefore risen from near the coldest to the warmest levels of the Holocene within the past century (**Figures 6 and 7**), reversing the long-term cooling trend that began ~3000 years ago.

During the past 46 years, Mediterranean SSTs have increased by ~1.54°C ± 0.09°C at an average warming rate of 0.33°C per decade. Prior to the ongoing Industrial-era warming, phases of rapid warming played out at 1070-705 B2K, 5350-4840 B2K and 8300-7150 B2K (**Figures 6 and 7**), although, as we highlight above, the tempo of warming rates during these periods contrast markedly with the recent Industrial period. For instance, average warming rates were (i) 0.021°C per decade during the Medieval Climate Anomaly (0.36 ± 0.15°C in 172 years), (ii) as low as 0.008°C per decade during the Holocene Warm Period (0.43 ± 0.17°C in 510 years) and (iii) 0.015°C per decade during the Holocene Climate Optimum (0.5 ± 0.2°C in 330 years). To test to what extent current warming rate is unparalleled in relation to the last 11,750 years, we calculated temperature changes using moving 46-years windows for the entire sequence (**Figure S9**). The 46-year window corresponds to the present ongoing phase of rapid Industrial-era warming (1973 to 2019); our

analysis confirms that the current rate of Mediterranean Sea warming is without precedent at the Holocene timescale.

These past warm periods are particularly relevant for modelling future changes in Mediterranean SSTs. Our reconstruction shows that Mediterranean SSTs have consistently exceeded the full distribution of Holocene warmth since 2011 (**Figure 7E**). If the rates of temperature increases observed over the past five decades were to remain constant for the rest of the twenty-first century, Mediterranean SSTs could attain anomalies of around 3.59 ± 0.08°C by 2100. This analysis suggests that Industrial-era Mediterranean SST warming rates are unprecedented at the scale of the Holocene, with Mediterranean SSTs projected to warm ~16 times faster than the closest analogue during the past ~11,000 years.

Conclusion

Our analysis provides further evidence that low carbon emissions are critical to mitigate contributions of Mediterranean SST increases to local and regional sea-level rise. Our multi-millennial assessment also clearly proves the need to assimilate pre-twentieth-century data into comprehensive assessments of industrial-era warming. At the scale of the Mediterranean, societal and economic impacts are likely to propagate in a nonlinear manner as climate-related hazards reach tipping points beyond which the affected physiological, anthropogenic, or ecological systems function less effectively or break down altogether. Many of these effects are likely to become even stronger in the near future because of the Mediterranean's growing human population levels and economic activity, particularly in coastal areas. Our analysis demonstrates that there are no direct Holocene analogues to assess the resilience of human societies in the face of such rapid current warming.

Acknowledgments

This work was supported by MITI CNRS Evénements rares (2022-2023) project AQUASANMARCO. We wish to thank an anonymous reviewer for constructive suggestions that helped to significantly improve earlier versions of the manuscript.

Figure and table captions

Figure 1: Location of the 54 records included in the Mediterranean database of SSTs. The numbers correspond to the references in Table 1.

Figure 2: Stack of Mediterranean Sea Surface Temperature (SST) anomalies for the Holocene. SST anomalies are the spatial average of the SST minus the mean of each individual time series in the database and are plotted on the B2K timescale. Change-point analysis was used to separate the time series into three periods: 11,750 to 9426 B2K (mu3 = -1.03), 9425 to 2951 B2K (mu2 = 0.32) and 2950 B2K to present (mu1 = 0.01). mu1-3 denote the averages for each statistically significant period. The light blue shading denotes the 68% Confidence Interval.

Figure 3: A. Mediterranean SSTs for the past ~10,000 years. **B.** Mediterranean SSTs plotted against June-July-August (JJA) insolation (orange line and shading) and December-January-February (DJF) insolation (green line and shading). **C.** Correlation between grouped SSTs and insolation for JJA and DJF. These analyses underline the role of changing Holocene seasonality in driving SST changes.

Figure 4: A. Mediterranean SST temperature anomalies (purple lines) plotted against Agassiz and Renland average temperature change record (in °C, green lines, record from Fisher et al., 2012) and Agassiz melt record (% melt, light-blue lines, record from Fisher et al., 2012). **B.** Grouped Mediterranean SST temperature anomalies versus grouped melting rates from the Agassiz record. The analysis demonstrates that increased meltwater inputs into the North Atlantic are correlated with cooling of Mediterranean SSTs.

Figure 5: Industrial-era warming compared and contrasted with other Holocene phases of rapid cooling (blue) or warming (orange).

Figure 6: A. Average annual rates of warming/cooling phases (in °C) for key Holocene periods. The analysis demonstrates that warming and cooling phases have been particularly rapid and of high amplitude during the past 1000 years. There are no direct Holocene analogues for the current rapid warming of Mediterranean SSTs. **B.** Onset and endpoints (dots) of key Holocene climate transitions (oblique lines) in Mediterranean SSTs. The vertical amplitude between the onset and the end of each

warming/cooling phase is in °C (positive for warming and negative for cooling), and represents the true T°C amplitude of change.

Figure 7: A-D. Industrial-era SST warming rates compared to other periods of rapid Holocene warming, including the Medieval Climate Anomaly (B), the Holocene Warm Period (C) and the Holocene Climate Optimum (D). **E**. Modelled Mediterranean SSTs up to 2100 based on current and, for comparison, Holocene warming rates. The data suggest that decadal warming rates are ~16 times greater than the closest Holocene analogue and that Mediterranean SSTs have persistently exceeded the full distribution of Holocene warmth since 2011.

Table 1: Basic metadata of the 54 records used in the Mediterranean SST compilation.

Supplementary figures

Figure S1: Location of the 54 records in the Mediterranean database, grouped by proxy type.

Figure S2: A. Temporal length and proxy type of the 54 records used to construct the Mediterranean SST stack. **B.** Number of records used in the Mediterranean SST stack through time.

Figure S3: A. Stack of Mediterranean Sea Surface Temperature (SST) anomalies for the Holocene, plotted on the B2K timescale. The light blue shading denotes the 68% Confidence Interval. The red line is a 200-year resampling, based on the coarsest chronological resolution of all the 2σ error margins used to construct the SST stack. The yellow line represents the 68% Confidence Interval associated with the 200-year time step. **B.** Same as (A) but excluding the annual resolution and associated Confidence Intervals.

Figure S4: Stack of Mediterranean Sea Surface Temperatures (SST) for the Holocene, plotted at 50-year intervals. The light blue error bars denote the 68% Confidence Intervals. The green error bars denote the average 2σ error of all records

used to reconstruct the SST record at time point x. The grey inset is a boxplot of the 2σ chronological errors in the initial 54 records (in years) used to construct the SST stack.

Figure S5: Comparison between SST minus mean average (cold colours) and SST spatial average (warm colours).

Figure S6: Potential role of geographic location in influencing the overall SST signal for the Holocene. **A.** Each SST record (West, Central and East Mediterranean) is presented as deviations from the mean. **B.** The number of sequences used per geographic location is shown as deviations from the mean. **C.** The weight of each geographic location in the final SST curve is subtracted (using **A.** x **B.**) and the resulting three curves (West, Central and East Mediterranean) are compared and contrasted with each other.

Figure S7: A. Mediterranean SST anomalies during the past 2000 years and broad climatic periods. The stars denote freezing events in the Bosphorus and cold winters in Istanbul, based on historical records (Yavuz et al., 2007). **B.** Short-time Fourier transform of the data highlighting the periods of marked climatic variability.

Figure S8: Boxplots of Mediterranean SST variability during the Holocene, highlighting the magnitude and rate of ongoing industrial-era warming. Recent warming contrasts markedly with long-term Holocene cooling of the Mediterranean Sea.

Figure S9: Holocene changes in Mediterranean SST°C using moving 46-years windows for the complete sequence. The 46-year window corresponds to the current phase of rapid Industrial-era warming (1973 to 2019). The first value covers the temperature rise between 1973 and 2019, the second between 1972 and 2018, the third between 1971 and 2017 and so forth for the entire sequence. The associated confidence interval comprises the average of the confidence intervals for each 46-yr time-span.

References

2019 Revision of World Population Prospects https://population.un.org/wpp/ Population Division of the Department of Economic and Social Affairs of the United Nations

Abram, N.J., McGregor, H.V., Tierney, J.E., Evans, M. N., McKay, N. P., Kaufman, D. S., the PAGES 2k Consortium, 2016. Early onset of industrial-era warming across the oceans and continents. Nature 536, 411-418.

Alexander, M. A., Scott, J. D., Friedland, K.D., Mills, K.E., Nyeⅱ, J.A., Pershing, A.J., Thomas, A.C., 2018. Projected sea surface temperatures over the 21st century: Changes in the mean, variability and extremes for large marine ecosystem regions of Northern Oceans. Elem. Sci. Anth. 6, 9.

Ausín, B., Flores, J., Sierro, F., Cacho, I., Hernández-Almeida, I., Martrat, B., Grimalt, J., 2015. Atmospheric patterns driving Holocene productivity in the Alboran Sea (Western Mediterranean): A multiproxy approach. The Holocene 25, 583-595.

Becker, K., Lipp, J., Versteegh, G., Wörmer, L., Hinrichs, K., 2015. Rapid and simultaneous analysis of three molecular sea surface temperature proxies and application to sediments from the Sea of Marmara. Organic Geochemistry 85, 42-53.

Blanchet, C., Frank, M., Schouten, S., 2014. Asynchronous Changes in Vegetation, Runoff and Erosion in the Nile River Watershed during the Holocene. PLoS ONE, 9, 115958.

Büntgen, U., Myglan, V.S., Charpentier Ljungqvist, F., McCormick, M., Di Cosmo, N., Sigl, M., Jungclaus, J., Wagner, S., Krusic, P.J., Esper, J., Kaplan, J. O., de Vaan, M.A.C., Luterbacher, J., Wacker, L., Tegel, W., Kirdyanov, A.V., 2016. Cooling and societal change during the Late Antique Little Ice Age from 536 to around 660 AD. Nature Geoscience 9, 231–236.

Cacho, I., Grimalt, J., Canals, M., Sbaffi, L., Shackleton, N., Schönfeld, J., Zahn, R., 2001. Variability of the western Mediterranean Sea surface temperature during the

last 25,000 years and its connection with the Northern Hemisphere climatic changes. Paleoceanography 16, 40-52.

Cacho, I., Grimalt, J., Pelejero, C., Canals, M., Sierro, F., Flores, J., Shackleton, N., 1999. Dansgaard-Oeschger and Heinrich event imprints in Alboran Sea paleotemperatures. Paleoceanography 14, 698-705.

Castañeda, I.S., Schefuß, E., Pätzold, J., Sinninghe Damsté, J.S., Weldeab, S., Schouten, S., 2010. Millennial-scale sea surface temperature changes in the eastern Mediterranean (Nile River Delta region) over the last 27,000 years. Paleoceanography 25, PA1208.

Català, A., Cacho, I., Frigola, J., Pena, L., Lirer, F., 2019. Holocene hydrography evolution in the Alboran Sea: a multi-record and multi-proxy comparison. Climate of the Past 15, 927-942.

Cisneros, M., Cacho, I., Frigola, J., Canals, M., Masqué, P., Martrat, B., Casado, M., Grimalt, J., Pena, L., Margaritelli, G., Lirer, F., 2016. Sea surface temperature variability in the central-western Mediterranean Sea during the last 2700 years: a multi-proxy and multi-record approach. Climate of the Past 12, 849-869.

Cramer, W., Guiot, J., Fader, M., Garrabou, J., Gattuso, J.-P., Iglesias, A., Lange, M. A., Lionello, P., Llasat, M.C., Paz, S., Peñuelas, J., Snoussi, M., Toreti, A., Tsimplis, M.N., Xoplaki, E., 2018. Climate change and interconnected risks to sustainable development in the Mediterranean. Nature Climate Change 8, 972-980.

Davtian, N., Ménot, G., Fagault, Y., Bard, E., 2019. Western Mediterranean Sea Paleothermometry Over the Last Glacial Cycle Based on the Novel RI-OH Index. Paleoceanography and Paleoclimatology 34, 616-634.

Doose, H. Rekonstruktion hydrographischer Verhältnisse im Californienstrom und im europäischen Mittelmeer zur Bildungszeit organisch kohlenstoffreicher Sedimente (GEOMAR Report, GEOMAR Research Center for Marine Geosciences, Christian Albrechts University in Kiel, 78, 1999).

EM-DAT, CRED / UCLouvain, Brussels, Belgium – www.emdat.be

Emeis, K., Dawson, A., 2003. Holocene palaeoclimate records over Europe and the North Atlantic. The Holocene 13, 305-309.

Emeis, K., Struck, U., Schulz, H., Rosenberg, R., Bernasconi, S., Erlenkeuser, H., Sakamoto, T., Martinez-Ruiz, F., 2000. Temperature and salinity variations of Mediterranean Sea surface waters over the last 16,000 years from records of planktonic stable oxygen isotopes and alkenone unsaturation ratios. Palaeogeography, Palaeoclimatology, Palaeoecology 158, 259-280.

Fischer, E.M., Schär, C., 2010. Consistent geographical patterns of changes in high-impact European heatwaves. Nature Geoscience 3, 398-403.

Fisher, D., Zheng, J., Burgess, D., Zdanowicz, C., Kinnard, C., Sharp, M., Bourgeois, J., 2012. Recent melt rates of Canadian arctic ice caps are the highest in four millennia. Global and Planetary Change 84-85, 3-7.

Fletcher, W.J., Debret, M., Fernanda Sanchez Goñi, M., 2013. Mid-Holocene emergence of a low- frequency millennial oscillation in western Mediterranean climate: Implications for past dynamics of the North Atlantic atmospheric westerlies. The Holocene 23, 153-166.

Giunta, S., Emeis, K.-C., Negri, A., 2001. Sea-surface temperature reconstruction of the last 16,000 years in the Eastern Mediterranean Sea. Rivista Italiana Di Paleontologia E Stratigrafia 107, 463-476.

Gogou, A., Triantaphyllou, M., Xoplaki, E., Izdebski, A., Parinos, C., Dimiza, M., Bouloubassi, I., Luterbacher, J., Kouli, K., Martrat, B., Toreti, A., Fleitmann, D., Rousakis, G., Kaberi, H., Athanasiou, M., Lykousis, V., 2016. Climate variability and socio-environmental changes in the northern Aegean (NE Mediterranean) during the last 1500 years. Quaternary Science Reviews 136, 209-228.

Guiot, J., Cramer, W., 2016. Climate change: The 2015 Paris Agreement thresholds and Mediterranean basin ecosystems. Science 354, 465-468.

Hughes, P.D., 2018. Little Ice Age glaciers and climate in the Mediterranean mountains: a new analysis. Geographical Research Letters 44, 15-45.

Incarbona, A., Martrat, B., Mortyn, P., Sprovieri, M., Ziveri, P., Gogou, A., Jordà, A., Xoplaki, E., Luterbacher, J., Langone, L., Marino, G., Rodríguez-Sanz, L., Triantaphyllou, M., Di Stefano, E., Grimalt, J., Tranchida, G., Sprovieri, R., Mazzola, S., 2016. Mediterranean circulation perturbations over the last five centuries: Relevance to past Eastern Mediterranean Transient-type events. Scientific Reports 6, 29623.

Jalali, B., Sicre, M., Bassetti, M., Kallel, N., 2016. Holocene climate variability in the North-Western Mediterranean Sea (Gulf of Lions). Climate of the Past 12, 91-101.

Kaniewski, D., Marriner, N., Cheddadi, R., Morhange, C., Ángel Cau Ontiveros, M., Fornós, J. J., Giaime, M., Trichona, V., Otto, T., Luce, F., Van Campo, E., 2020. Recent anthropogenic climate change exceeds the rate and magnitude of natural Holocene variability on the Balearic Islands. Anthropocene 32, 100268.

Kaniewski, D., Marriner, N., Cheddadi, R., Morhange, C., Bretschneider, J., Jans, G., Otto, T., Luce, F., Van Campo, E., 2019. Cold and dry outbreaks in the eastern Mediterranean 3200 years ago. Geology 47, 933-937.

Kaniewski, D., Marriner, N., Ilan, D., Morhange, C., Thareani, Y., Van Campo, E., 2017. Climate change and water management in the Biblical city of Dan. Science Advances 3, e1700954.

Kaniewski, D., Van Campo, E., Guiot, J., Le Burel, S., Otto, T., Baeteman, C., 2013. Environmental Roots of the Late Bronze Age Crisis. PLoS ONE 8, e71004.

Kim, J., Schouten, S., Rodrigo-Gámiz, M., Rampen, S., Marino, G., Huguet, C., Helmke, P., Buscail, R., Hopmans, E., Pross, J., Sangiorgi, F., Middelburg, J.,

Sinninghe Damsté, J., 2015. Influence of deep-water derived isoprenoid tetraether lipids on the TEX86H paleothermometer in the Mediterranean Sea. Geochimica et Cosmochimica Acta 150, 125-141.

Laskar, J., Fienga, A., Gastineau, M., Manche, H., 2011. La2010: A new orbital solution for the long-term motion of the Earth. Astron. Astrophys. 532, A89.

Lecavalier, B.S., Fisher, D.A., Milne, G.A., Vinther, B.M., Tarasov, L., Huybrechts, P., Lacelle, D., Main, B., Zheng, J., Bourgeois, J., Dyke, A. S., 2017. High Arctic Holocene temperature record from the Agassiz ice cap and Greenland ice sheet evolution. PNAS 114, 5952-5957.

Lionello, P., Scarascia, L., 2018. The relation between climate change in the Mediterranean region and global warming. Reg. Environ. Change 18, 1481–1493.

Macias, D., Garcia-Gorriz, E., Stips, A., 2013. Understanding the causes of recent warming in Mediterranean waters. How much could be attributed to climate change? PLoS ONE 8, e81591.

Martrat, B., Grimalt, J., Lopez-Martinez, C., Cacho, I., Sierro, F., Flores, J., Zahn, R., Canals, M., Curtis, J., Hodell, D., 2004. Abrupt Temperature Changes in the Western Mediterranean over the Past 250,000 Years. Science 306, 1762-1765.

Martrat, B., Grimalt, J., Shackleton, N., de Abreu, L., Hutterli, M., Stocker, T., 2007. Four Climate Cycles of Recurring Deep and Surface Water Destabilizations on the Iberian Margin. Science 317, 502-507.

Martrat, B., Jimenez-Amat, P., Zahn, R., Grimalt, J., 2014. Similarities and dissimilarities between the last two deglaciations and interglaciations in the North Atlantic region. Quaternary Science Reviews 99, 122-134.

McGregor, H.V., Evans, M.N., Goosse, H., Leduc, G., Martrat, B., Addison, J.A., Mortyn, P.G., Oppo, D.W., Seidenkrantz, M.-S., Sicre, M.-A., Phipps, S. J., Selvaraj,

575 K., Thirumalai, K., Filipsson, H.L., Ersek, V., 2015. Robust global ocean cooling trend for the pre-industrial Common Era. Nature Geoscience 8, 671–677.

Moreno, A., Pérez, A., Frigola, J., Nieto-Moreno, V., Rodrigo-Gámiz, M., Martrat, B., González-Sampériz, P., Morellón, M., Martín-Puertas, C., Corella, J., Belmonte, Á.,
580 Sancho, C., Cacho, I., Herrera, G., Canals, M., Grimalt, J., Jiménez-Espejo, F., Martínez-Ruiz, F., Vegas-Vilarrúbia, T., Valero-Garcés, B., 2012. The Medieval Climate Anomaly in the Iberian Peninsula reconstructed from marine and lake records. Quaternary Science Reviews 43, 16-32.

585 Nieto-Moreno, V., Martínez-Ruiz, F., Willmott, V., García-Orellana, J., Masqué, P., Sinninghe Damsté, J., 2013. Climate conditions in the westernmost Mediterranean over the last two millennia: An integrated biomarker approach. Organic Geochemistry 55, 1-10.

590 NOAA National Centers for Environmental information, Climate at a Glance: Global Time Series, published December 2020, retrieved on January 7, 2021 from https://www.ncdc.noaa.gov/cag/

Pastor, F., Valiente, J.A., Palau, J.L., 2018. Sea Surface Temperature in the
595 Mediterranean: Trends and Spatial Patterns (1982–2016). Pure and Applied Geophysics 175, 4017-4029.

Peyron, O., Combourieu-Nebout, N., Brayshaw, D., Goring, S., Andrieu-Ponel, V., Desprat, S., Fletcher, W., Gambin, B., Ioakim, C., Joannin, S., Kotthoff, U., Kouli, K.,
600 Montade, V., Pross, J., Sadori, L., Magny, M., 2017. Precipitation changes in the Mediterranean basin during the Holocene from terrestrial and marine pollen records: a model–data comparison. Climate of the Past 13, 249-265.

Peyron, O., Goring, S., Dormoy, I., Kotthoff, U., Pross, J., de Bealieu, J.L., Drescher-
605 Schneider, R., Magny, M., 2011. Holocene seasonality changes in the central Mediterranean region reconstructed from the pollen sequences of Lake Accesa (Italy) and Tenaghi Philippon (Greece). The Holocene 21, 131-146.

Rodrigo-Gámiz, M., Martínez-Ruiz, F., Rampen, S., Schouten, S., Sinninghe Damsté, J., 2014. Sea surface temperature variations in the western Mediterranean Sea over the last 20 kyr: A dual-organic proxy (UK′ 37 and LDI) approach. Paleoceanography 29, 87-98.

Shaw, I., 2004. The Oxford History of Ancient Egypt. Oxford University Press, Oxford.

Schirrmacher, J., Weinelt, M., Blanz, T., Andersen, N., Salgueiro, E., Schneider, R., 2019. Multi-decadal atmospheric and marine climate variability in southern Iberia during the mid- to late-Holocene. Climate of the Past 15, 617-634.

Schneider, T., Bischoff, T., Haug, G.H., 2014. Migrations and dynamics of the intertropical convergence zone. Nature 513, 45–53.

Siani, G., Magny, M., Paterne, M., Debret, M., Fontugne, M., 2013. Paleohydrology reconstruction and Holocene climate variability in the South Adriatic Sea. Climate of the Past 9, 499-515.

Sinha, A., Kathayat, G., Weiss, H., Li, H., Cheng, H., Reuter, J., Schneider, A.W., Berkelhammer, M., Adali, S.F., Stott, L.D., Lawrence Edwards, R., 2019. Role of climate in the rise and fall of the neo-assyrian empire. Science Advances 5, aax6656.

Tramblay, Y., Koutroulis, A., Samaniego, L., Vicente-Serrano, S.M., Volaire, F., Boone, A., Le Page, M., Carmen Llasat, M., Albergel, C., Burak, S., Cailleret, M., Cindrić Kalin, K., Davi, H., Dupuy, J.-L., Greve, P., Grillakis, M., Hanich, L., Jarlan, L., Martin-StPaul, N., Martínez-Vilalta, J., Mouillot, F., Pulido-Velazquez, D., Quintana-Seguí, P., Renard, D., Turco, M., Türkeş, M., Trigo, R., Vidal, J.-P., Vilagrosa, A., Zribi, M., Polcher, J., 2020. Challenges for drought assessment in the Mediterranean region under future climate scenarios. Earth-Science Reviews 210, 103348.

Tuel, A., Eltahir, E.A.B., 2020. Why Is the Mediterranean a Climate Change Hot Spot? Journal of Climate 33, 5829–5843.

Vacchi, M., Joyse, K., Kopp, R., Marriner, N., Kaniewski, D., Rovere, A., 2021. Climate pacing of millennial sea-level change variability in the central and western Mediterranean. Nature Communications 12, 4013.

Versteegh, G., de Leeuw, J., Taricco, C., Romero, A., 2007. Temperature and productivity influences on $U_{37}^{K'}$ and their possible relation to solar forcing of the Mediterranean winter. Geochemistry, Geophysics, Geosystems 8, Q09005.

Weiss, H., 2016. Global megadrought, societal collapse and resilience at 4.2–3.9ka BP across the Mediterranean and west Asia. Pages Magazine 24, 62-63.

Woodruff, S.D., Worley, S.J., Lubker, S.J., Ji, Z., Freeman, J.E., Berry, D.I., Brohan, P., Kent, E.C., Reynolds, R.W., Smith, S.R., Wilkinson, C., 2011. ICOADS Release 2.5: extensions and enhancements to the surface marine meteorological archive. International Journal of Climatology 31, 951-967.

Yavuz, V., Akçar, N., Schlüchter, C., 2007. in The Black Sea Flood Question: Changes in Coastline, Climate, and Human Settlement (eds Yanko-Hombach, V., Gilbert, A. S., Panin, N., Dolukhanov, P. M.) 633–649 (Springer).

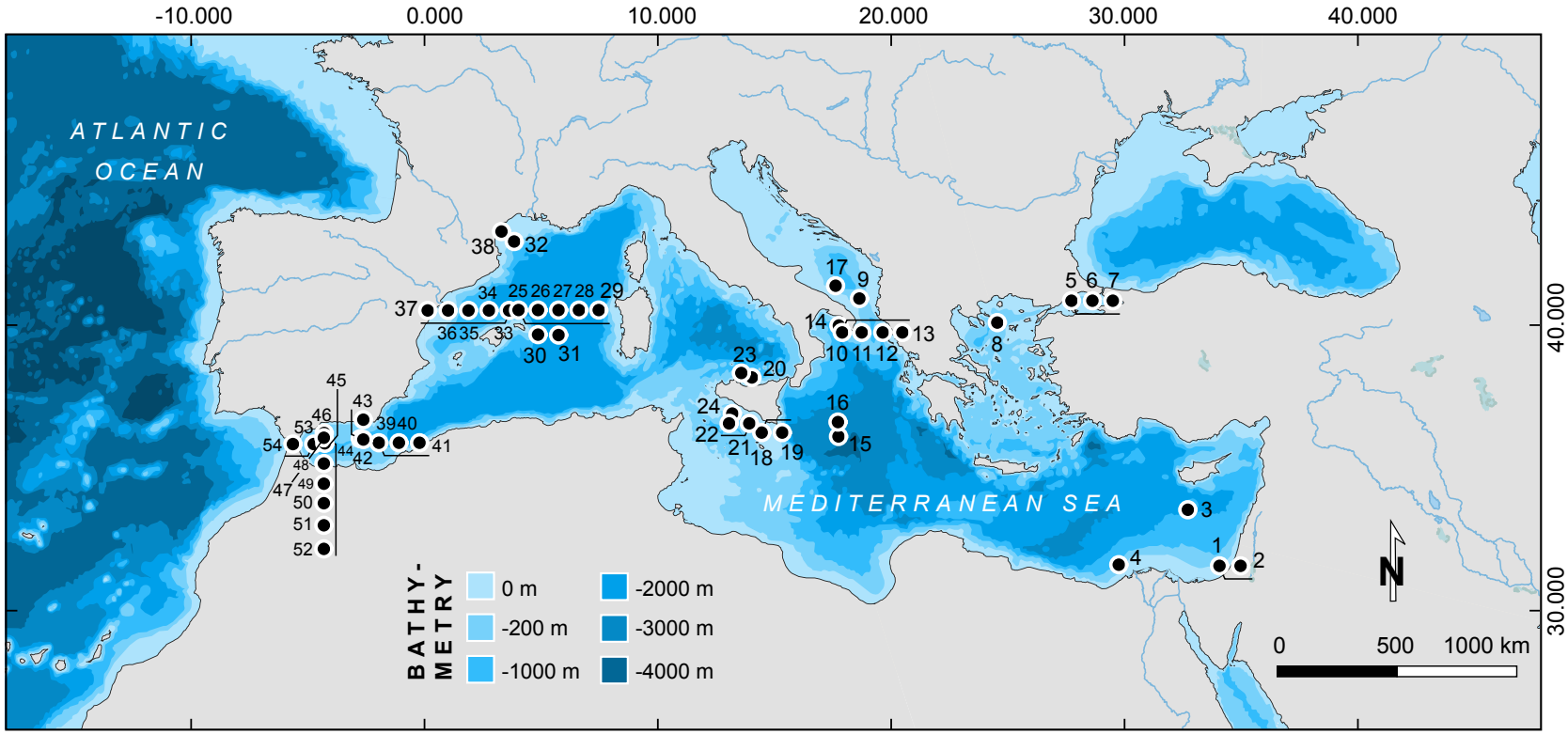
-10.000
0.000
10.000
20.000
30.000
40.000
40.000
30.000
ATLANTIC
OCEAN
MEDITERRANEAN SEA
BATHY-
METRY
0 m
-200 m
-1000 m
-2000 m
-3000 m
-4000 m
0
500
1000 km
N
1
2
3
4
5
6
7
8
9
10
11
12
13
14
15
16
17
18
19
20
21
22
23
24
25
26
27
28
29
30
31
32
33
34
35
36
37
38
39
40
41
42
43
44
45
46
47
48
49
50
51
52
53
54

Figure 1

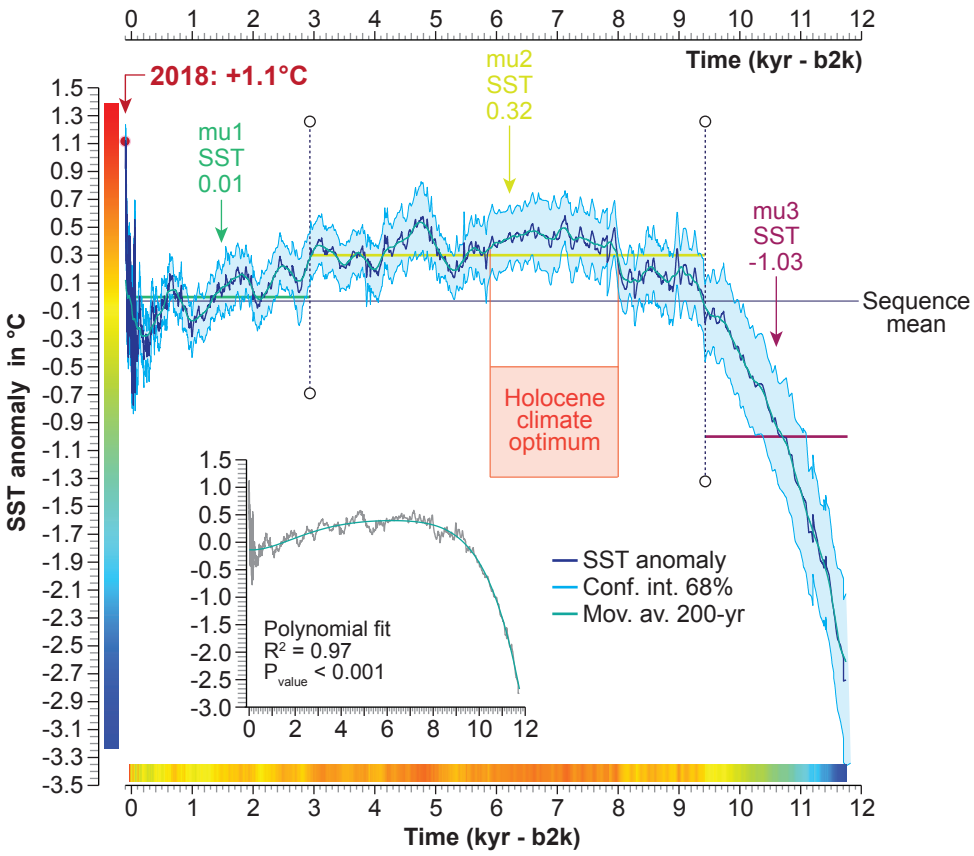
Time (kyr - b2k)
2018: +1.1°C
mu1
SST
0.01
mu2
SST
0.32
mu3
SST
-1.03
Sequence
mean
Holocene
climate
optimum
SST anomaly in °C
Polynomial fit
R² = 0.97
P value < 0.001
SST anomaly
Conf. int. 68%
Mov. av. 200-yr
Time (kyr - b2k)

Figure 2

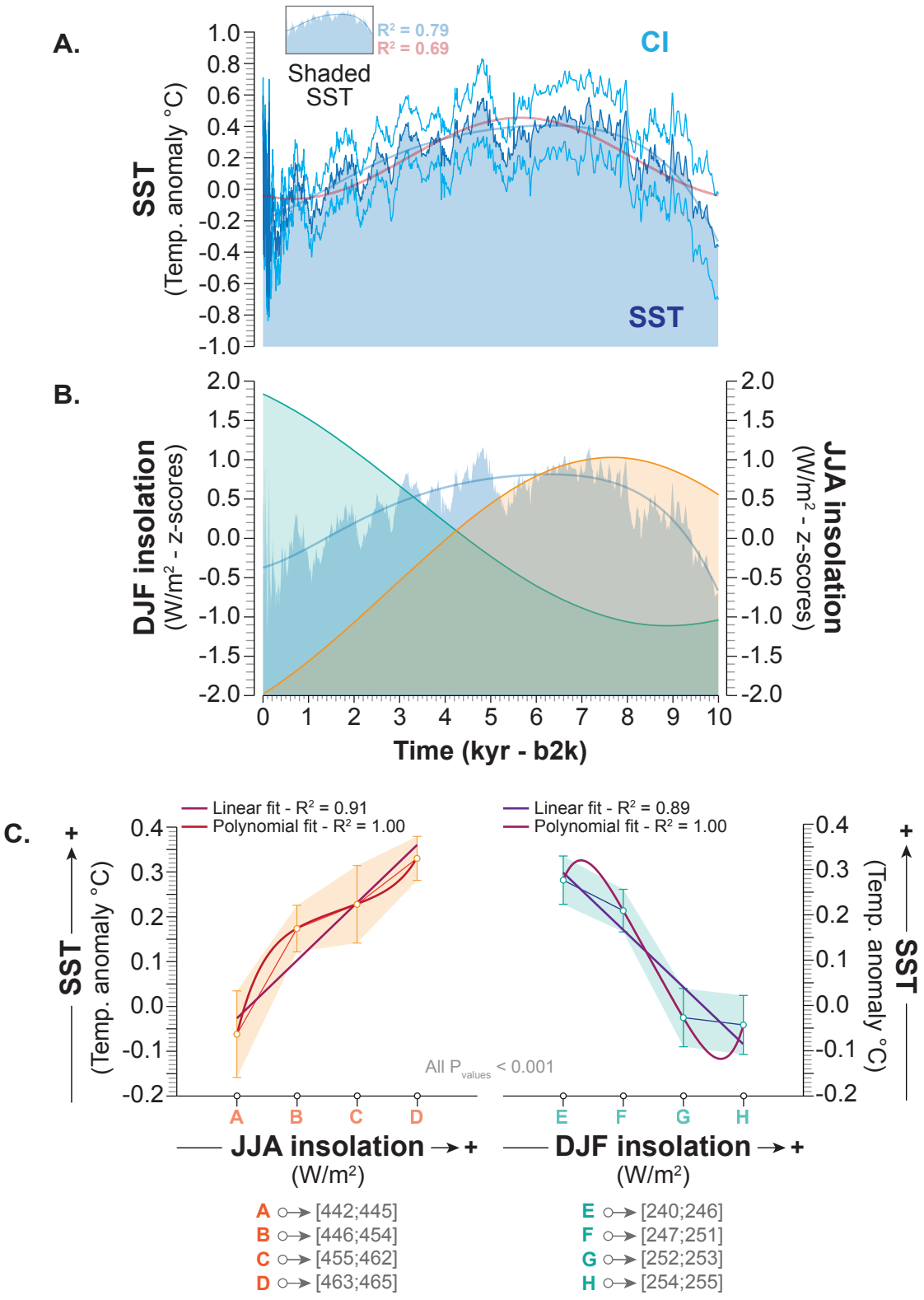
A.
R² = 0.79
R² = 0.69
Shaded SST
CI
SST
SST (Temp. anomaly °C)
B.
DJF insolation (W/m² - z-scores)
JJA insolation (W/m² - z-scores)
Time (kyr - b2k)
C.
Linear fit - R² = 0.91
Polynomial fit - R² = 1.00
Linear fit - R² = 0.89
Polynomial fit - R² = 1.00
All P values < 0.001
JJA insolation → + (W/m²)
DJF insolation → + (W/m²)
A → [442;445]
B → [446;454]
C → [455;462]
D → [463;465]
E → [240;246]
F → [247;251]
G → [252;253]
H → [254;255]

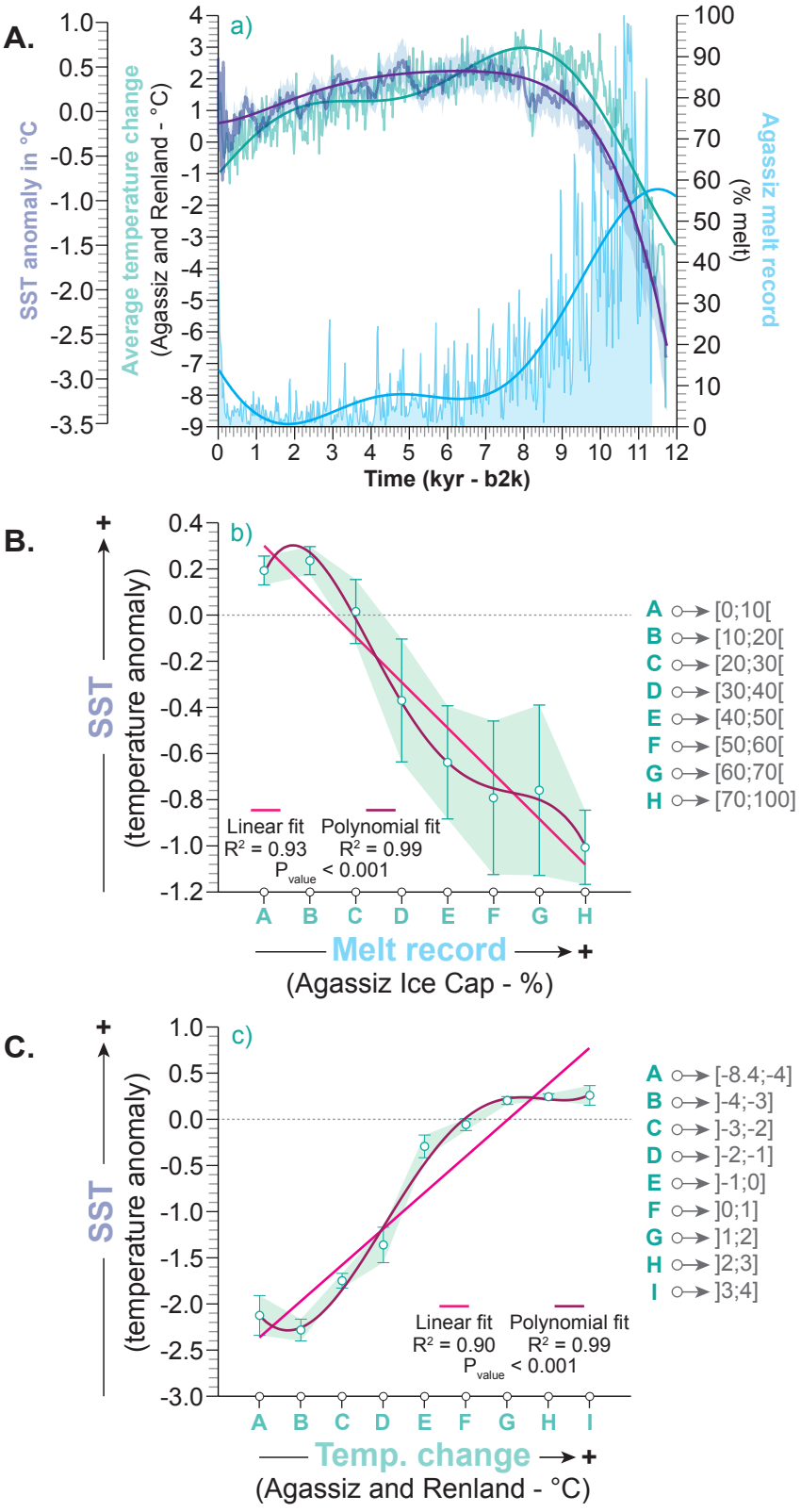
A.
a)
SST anomaly in °C
Average temperature change
(Agassiz and Renland - °C)
Agassiz melt record
(% melt)
Time (kyr - b2k)
B.
b)
SST
(temperature anomaly)
Linear fit
R² = 0.93
Polynomial fit
R² = 0.99
P value < 0.001
A → [0;10[
B → [10;20[
C → [20;30[
D → [30;40[
E → [40;50[
F → [50;60[
G → [60;70[
H → [70;100]
Melt record
(Agassiz Ice Cap - %)
C.
c)
SST
(temperature anomaly)
Linear fit
R² = 0.90
Polynomial fit
R² = 0.99
P value < 0.001
A → [-8.4;-4]
B →]-4;-3]
C →]-3;-2]
D →]-2;-1]
E →]-1;0]
F →]0;1]
G →]1;2]
H →]2;3]
I →]3;4]
Temp. change
(Agassiz and Renland - °C)

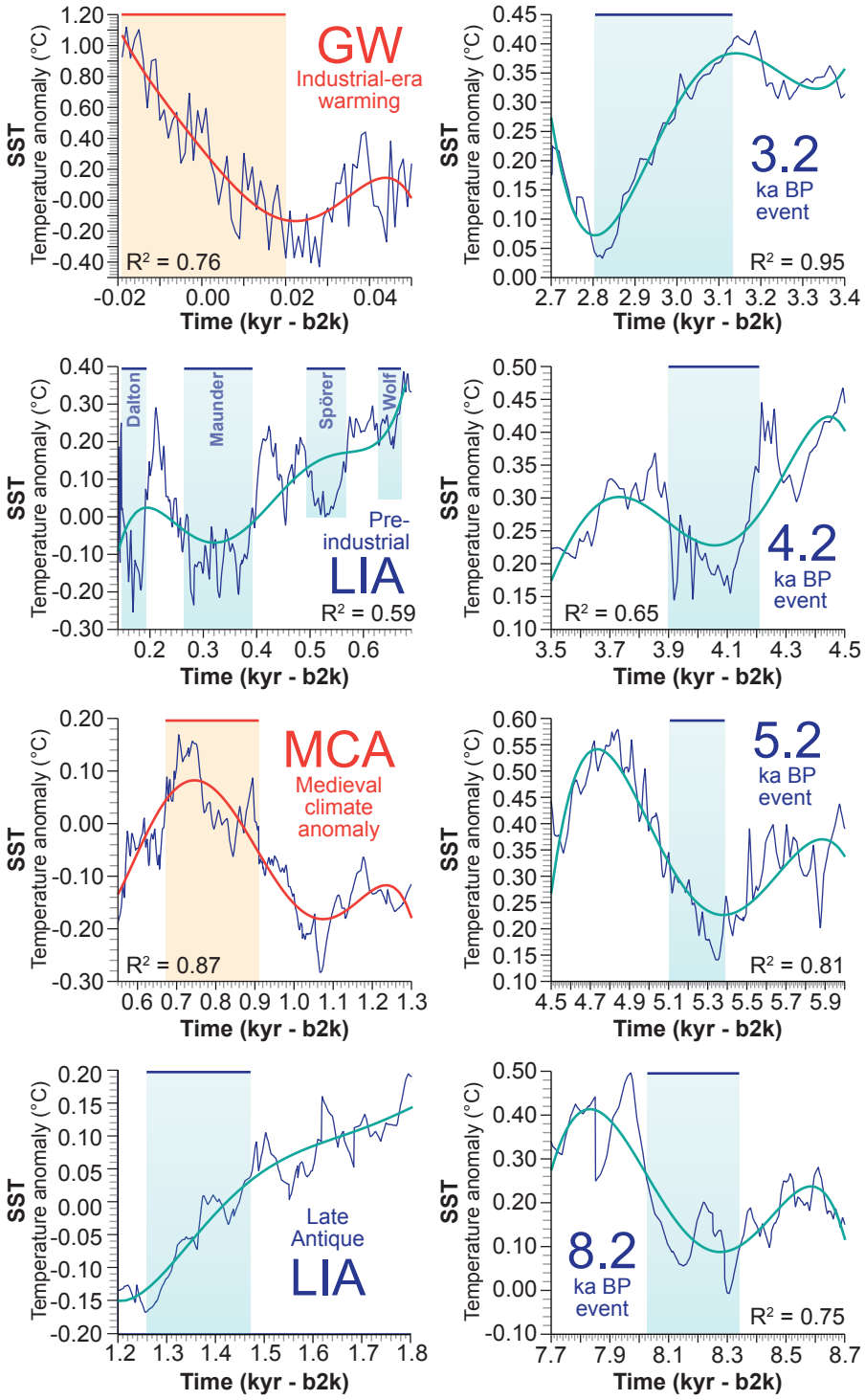
GW
Industrial-era warming
R² = 0.76
3.2
ka BP event
R² = 0.95
Dalton
Maunder
Spörer
Wolf
Pre-industrial
LIA
R² = 0.59
4.2
ka BP event
R² = 0.65
MCA
Medieval climate anomaly
R² = 0.87
5.2
ka BP event
R² = 0.81
Late Antique
LIA
8.2
ka BP event
R² = 0.75
SST
Temperature anomaly (°C)
Time (kyr - b2k)

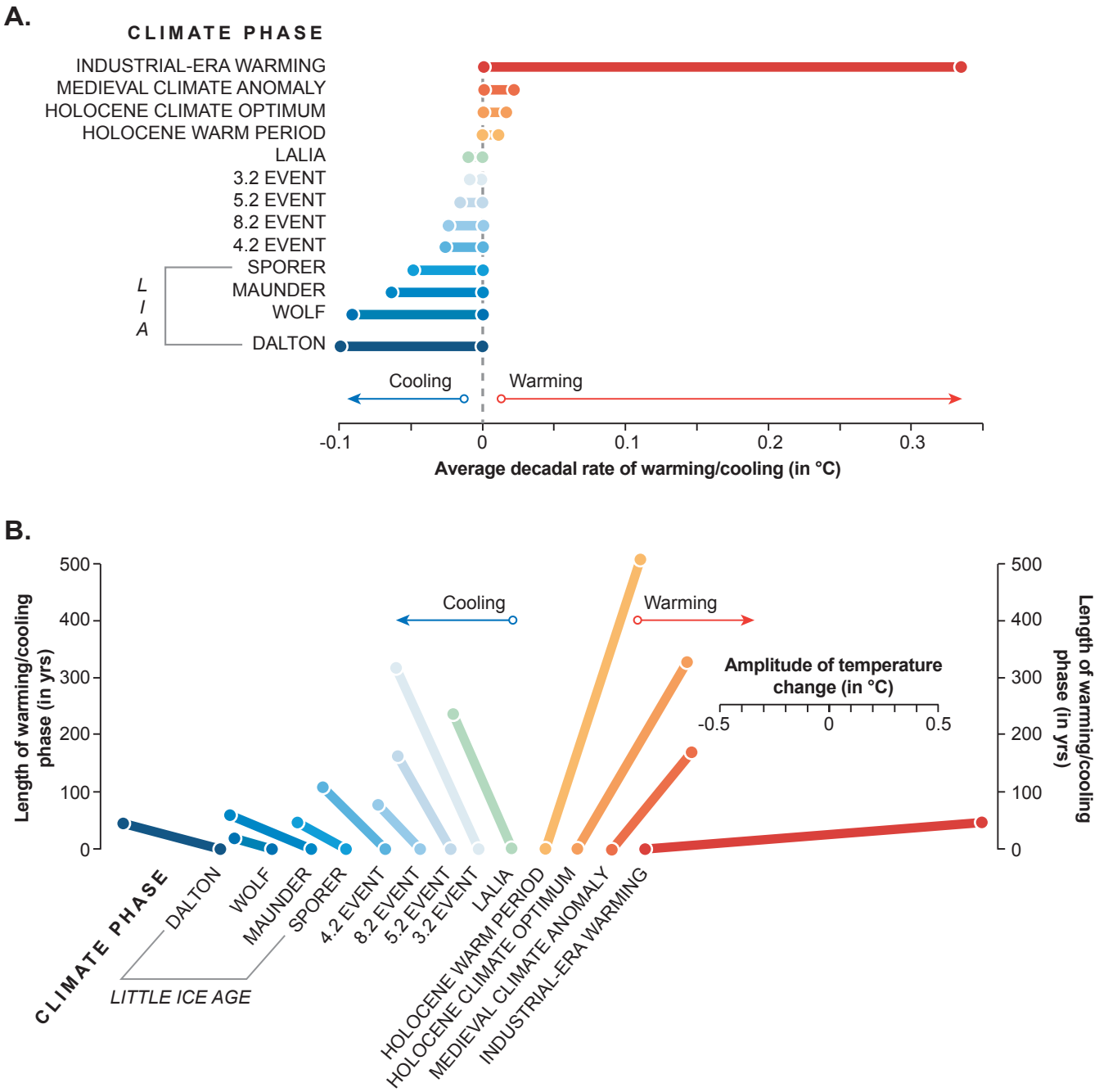
A.
CLIMATE PHASE
INDUSTRIAL-ERA WARMING
MEDIEVAL CLIMATE ANOMALY
HOLOCENE CLIMATE OPTIMUM
HOLOCENE WARM PERIOD
LALIA
3.2 EVENT
5.2 EVENT
8.2 EVENT
4.2 EVENT
SPORER
MAUNDER
WOLF
DALTON
LIA
Cooling
Warming
-0.1
0
0.1
0.2
0.3
Average decadal rate of warming/cooling (in °C)
B.
Length of warming/cooling phase (in yrs)
500
400
300
200
100
0
Cooling
Warming
Amplitude of temperature change (in °C)
-0.5
0
0.5
CLIMATE PHASE
DALTON
WOLF
MAUNDER
SPORER
4.2 EVENT
8.2 EVENT
5.2 EVENT
3.2 EVENT
LALIA
HOLOCENE WARM PERIOD
HOLOCENE CLIMATE OPTIMUM
MEDIEVAL CLIMATE ANOMALY
INDUSTRIAL-ERA WARMING
LITTLE ICE AGE

Figure 6

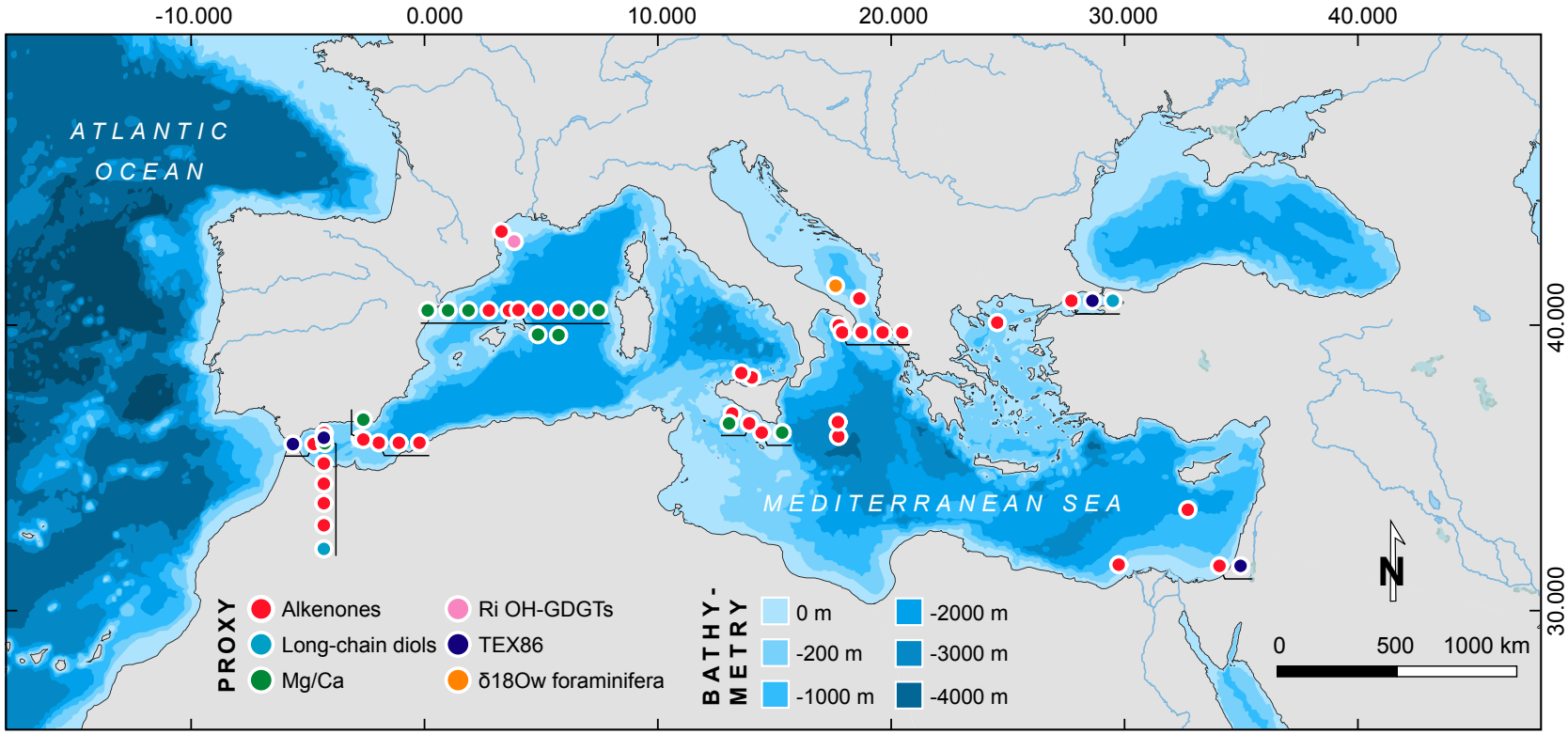

Figure S1: Location of the 54 records in the Mediterranean database, grouped by proxy type.

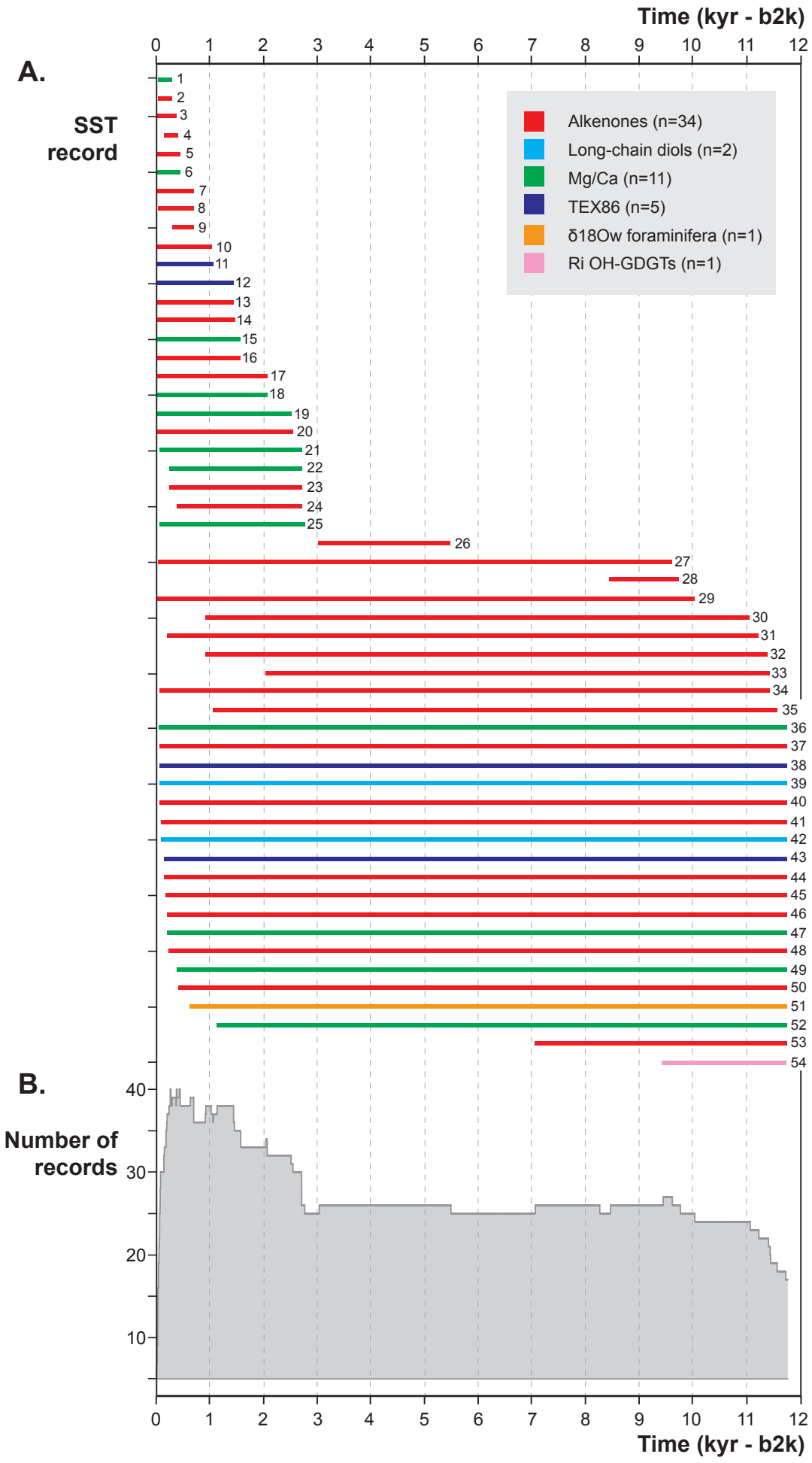

Figure S2: A. Temporal length and proxy type of the 54 records used to construct the Mediterranean SST stack. B. Number of records used in the Mediterranean SST stack through time.

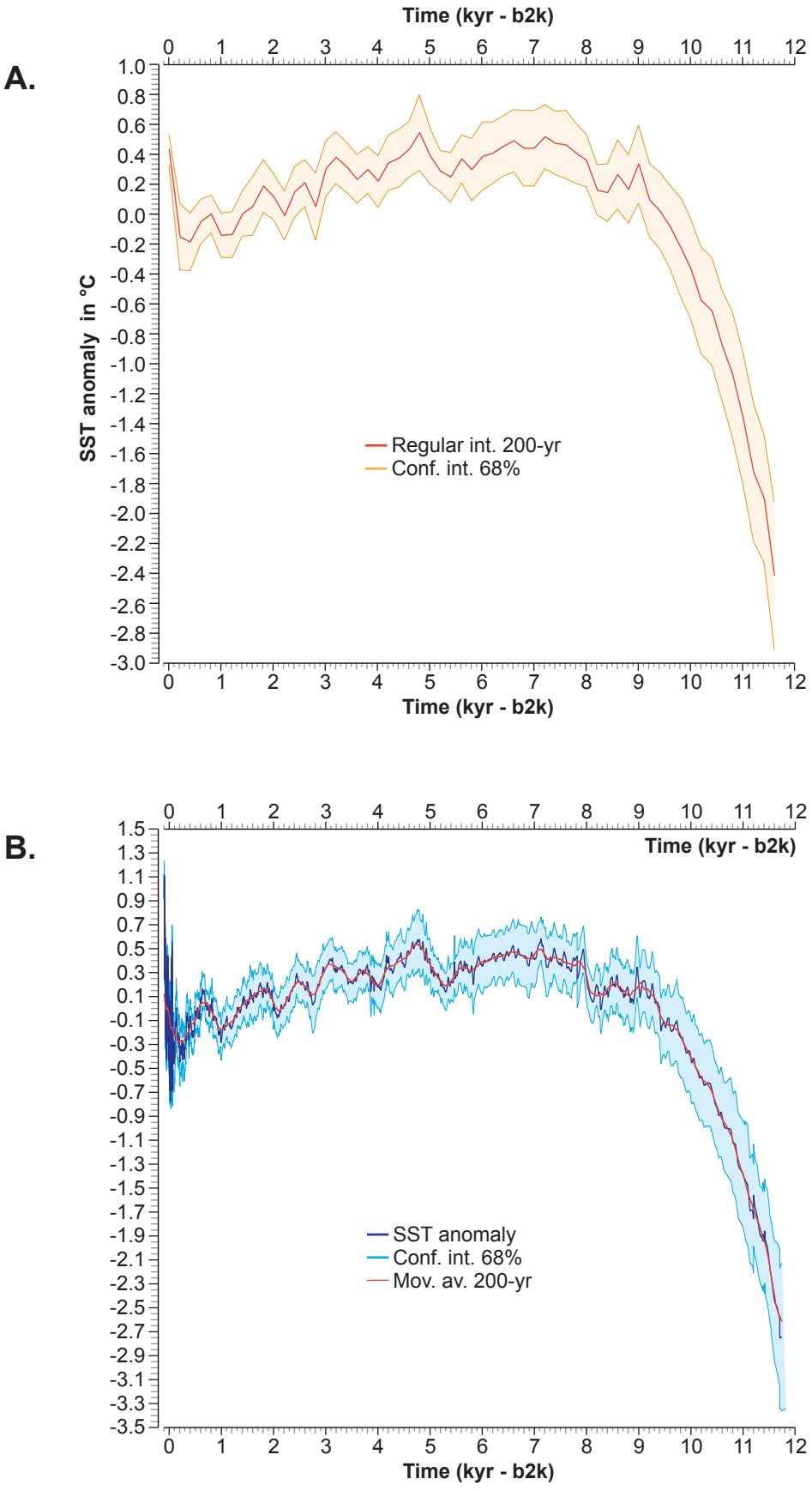

Figure S3: A. Stack of Mediterranean Sea Surface Temperature (SST) anomalies for the Holocene, plotted on the B2K timescale. The light blue shading denotes the 68% Confidence Interval. The red line is a 200-year resampling, based on the coarsest chronological resolution of all the 2σ error margins used to construct the SST stack. The yellow line represents the 68% Confidence Interval associated with the 200-year time step. B. Same as (A) but excluding the annual resolution and associated Confidence Intervals.

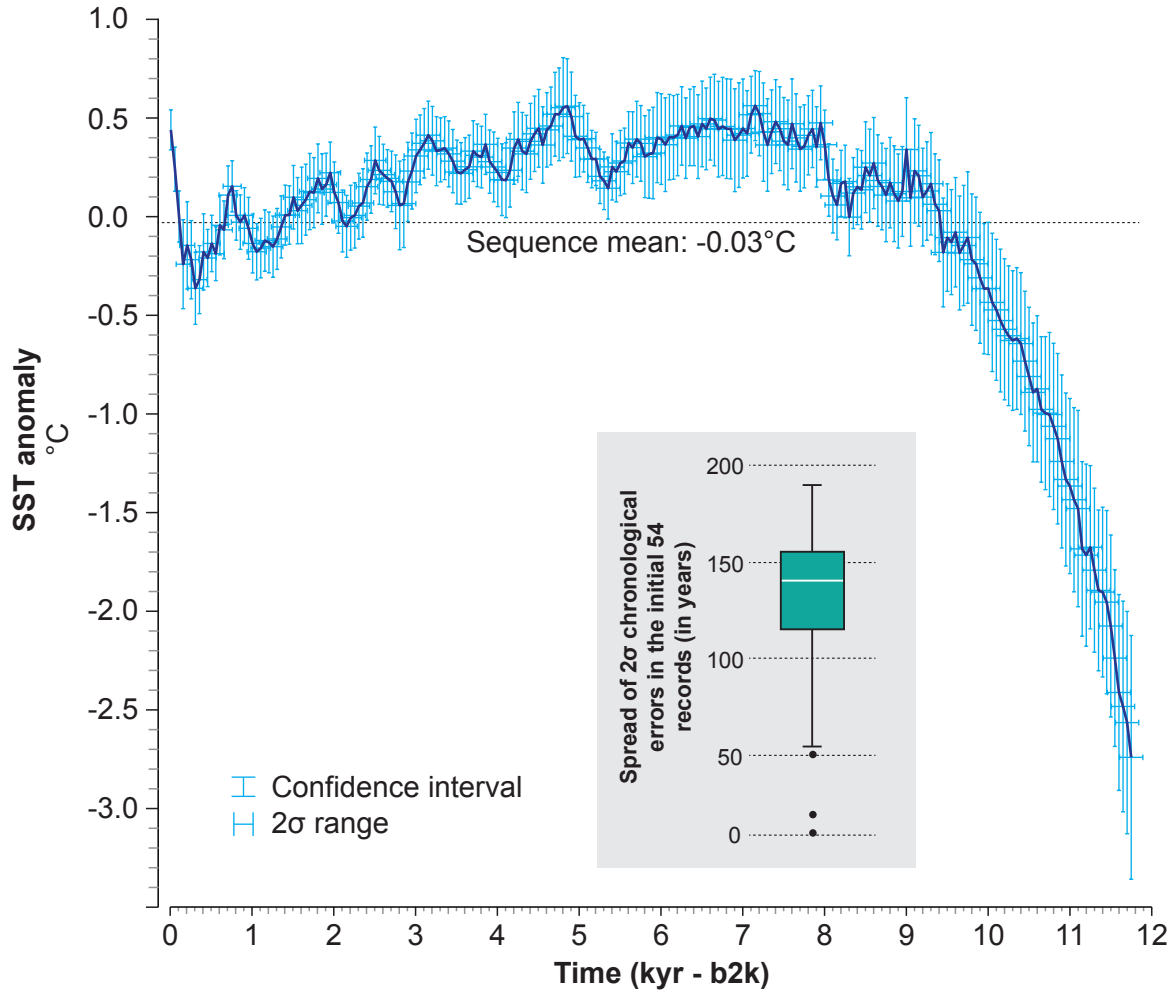

Figure S4: Stack of Mediterranean Sea Surface Temperatures (SST) for the Holocene, plotted at 50-year intervals. The light blue error bars denote the 68% Confidence Intervals. The green error bars denote the average 2σ error of all records used to reconstruct the SST record at time point x. The grey inset is a boxplot of the 2σ chronological errors in the initial 54 records (in years) used to construct the SST stack.

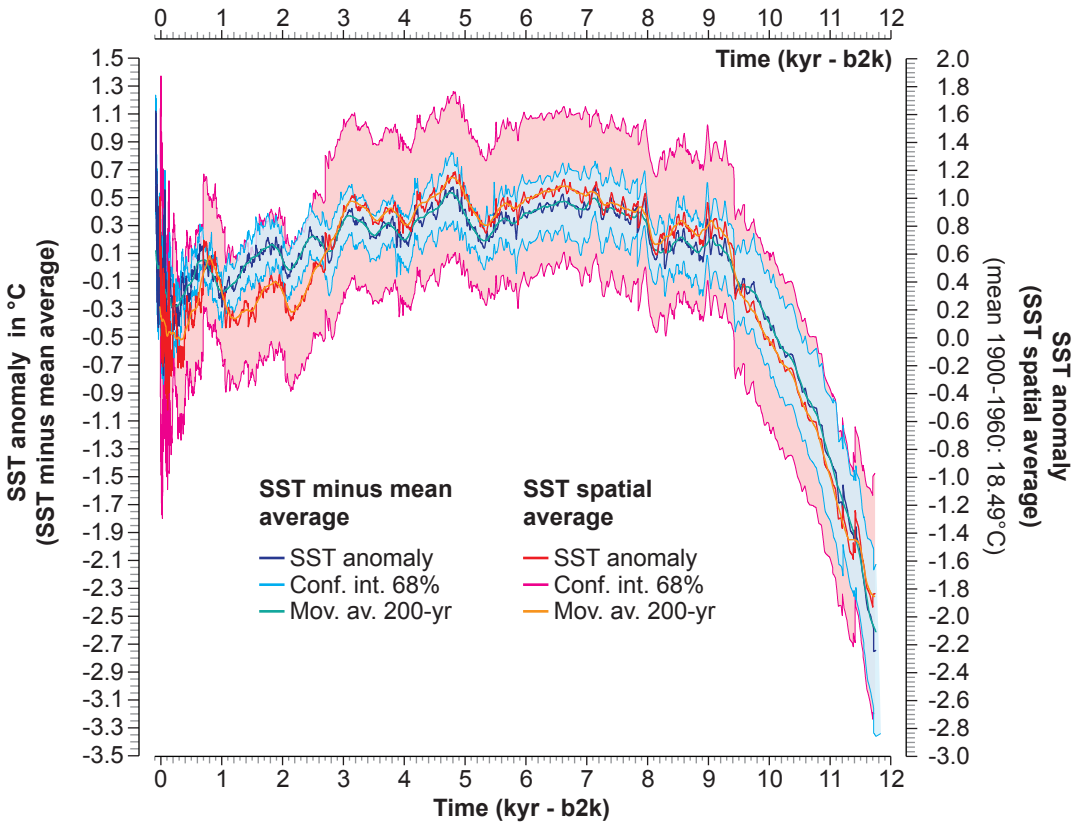

Figure S5: Comparison between SST minus mean average (cold colours) and SST spatial average (warm colours).

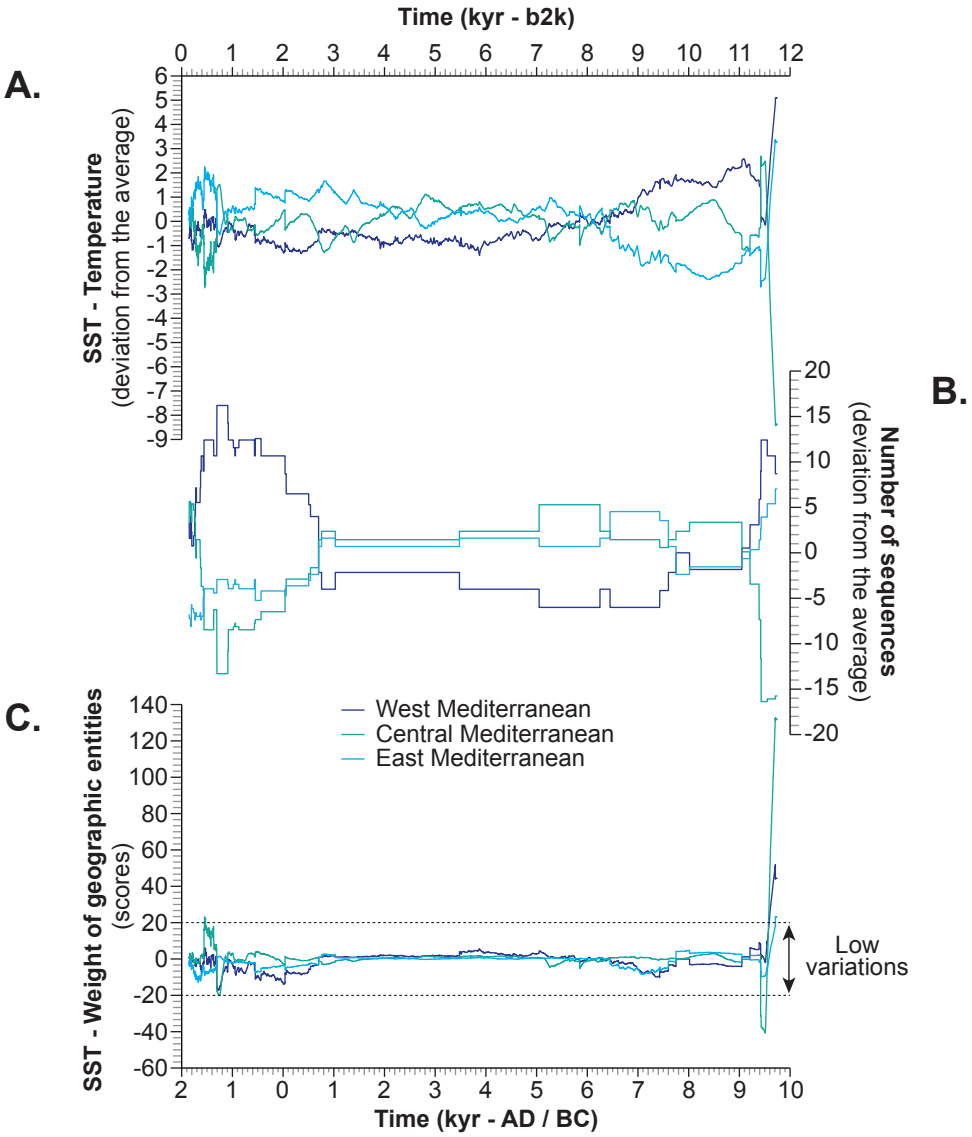

Figure S6: Potential role of geographic location in influencing the overall SST signal for the Holocene. A. Each SST record (West, Central and East Mediterranean) is presented as deviations from the mean. B. The number of sequences used per geographic location is shown as deviations from the mean. C. The weight of each geographic location in the final SST curve is subtracted (using A. x B.) and the resulting three curves (West, Central and East Mediterranean) are compared and contrasted with each other.

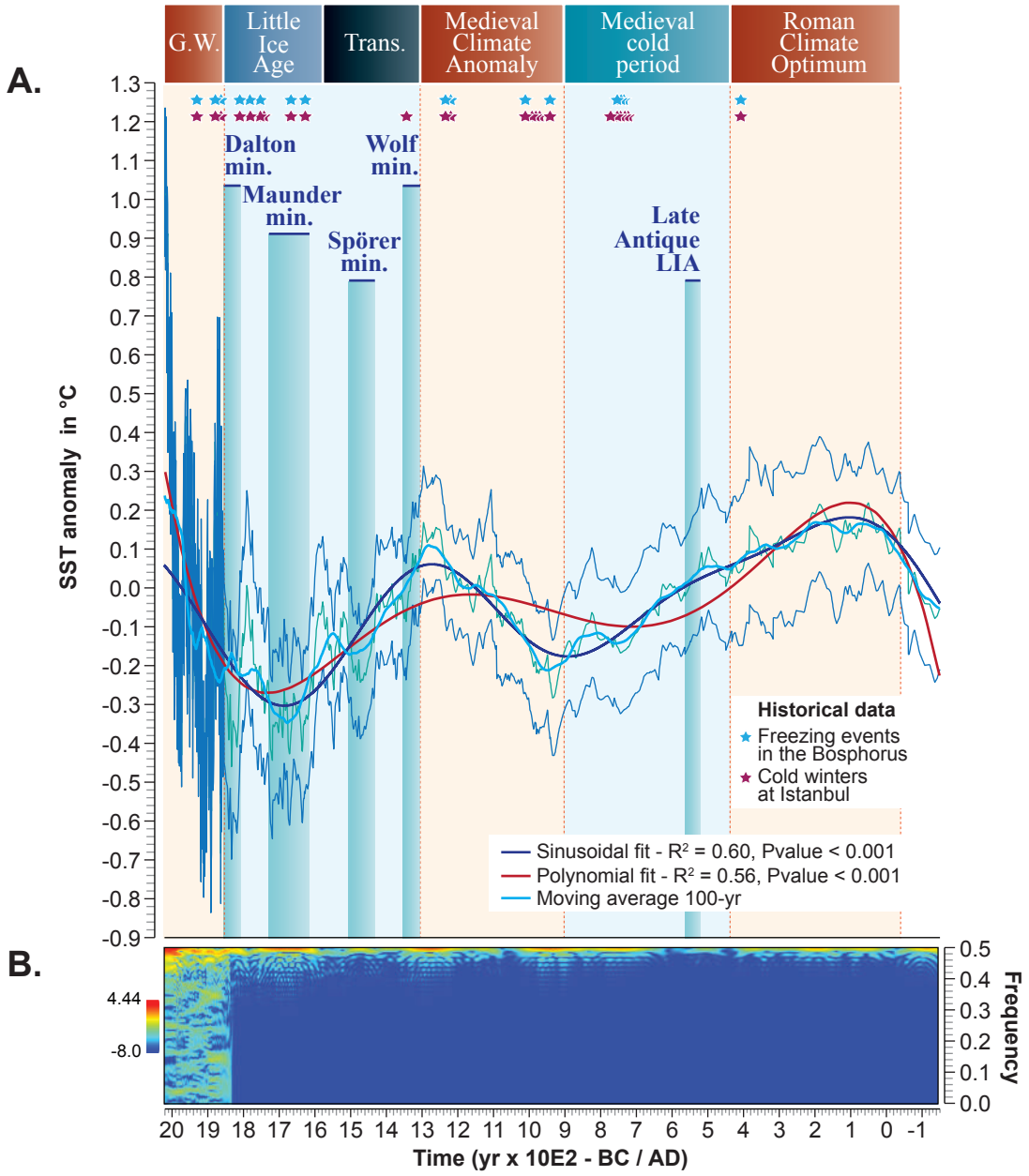

Figure S7: A. Mediterranean SST anomalies during the past 2000 years and broad climatic periods. The stars denote freezing events in the Bosphorus and cold winters in Istanbul, based on historical records (Yavuz et al., 2007). B. Short-time Fourier transform of the data highlighting the periods of marked climatic variability.

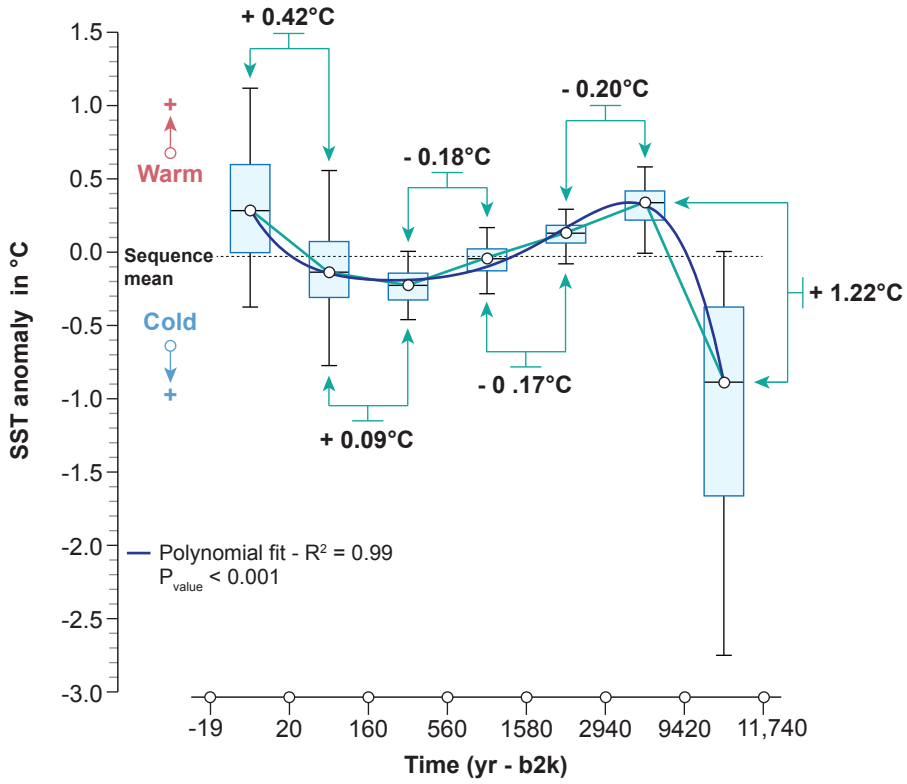

Figure S8: Boxplots of Mediterranean SST variability during the Holocene, highlighting the magnitude and rate of ongoing industrial-era warming. Recent warming contrasts markedly with long-term Holocene cooling of the Mediterranean Sea.

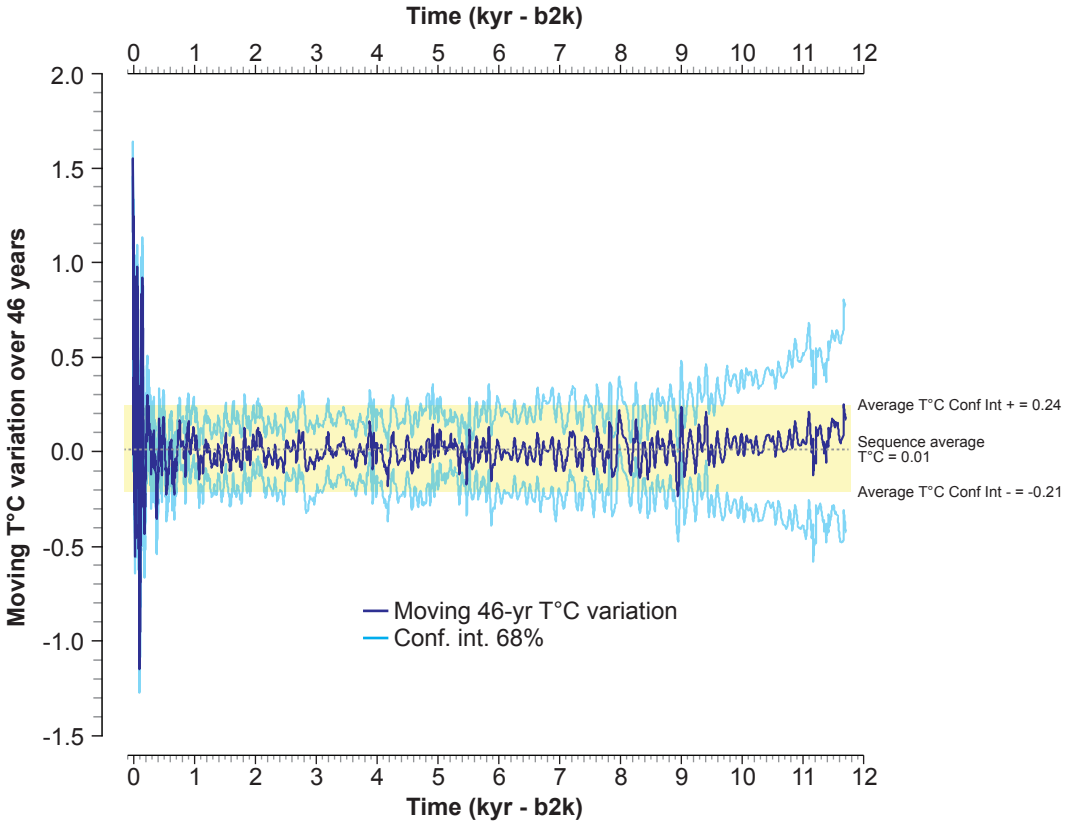

Figure S9: Holocene changes in Mediterranean SST°C using moving 46-years windows for the complete sequence. The 46-year window corresponds to the current phase of rapid Industrial-era warming (1973 to 2019). The first value covers the temperature rise between 1973 and 2019, the second between 1972 and 2018, the third between 1971 and 2017 and so forth for the entire sequence. The associated confidence interval comprises the average of the confidence intervals for each 46-yr time-span.